

## Observational Study of Marine Atmospheric Boundary Layer Characteristics during Swell

A. SMEDMAN, U. HÖGSTRÖM, AND E. SAHLEÉ

*Department of Earth Sciences, Uppsala University, Uppsala, Sweden*

W. M. DRENNAN

*Rosenstiel School of Marine and Atmospheric Science, University of Miami, Miami, Florida*

K. K. KAHMA AND H. PETERSSON

*Finnish Institute of Marine Research, Helsinki, Finland*

F. ZHANG

*Rosenstiel School of Marine and Atmospheric Science, University of Miami, Miami, Florida*

(Manuscript received 16 September 2008, in final form 9 March 2009)

### ABSTRACT

By combining simultaneous data from an instrumented Air–Sea Interaction Spar (ASIS) buoy and a 30-m tower, profiles of wind and turbulence characteristics have been obtained at several heights from about 1 to 30 m above the water surface during swell conditions. Five cases formed as averages over time periods ranging from 2.5 to 9.5 h, representing quasi-steady conditions, have been selected. They represent a range of typical wave age and include wind-following swell cases and cross-swell cases. For relatively large wave age, the wind profile exhibits a well-defined maximum in the height range 5–10 m; for more modest wave age, this maximum turns into a sharp “knee” in the wind profile. Below the maximum (or knee), the wind increases rapidly with height; above that point the wind is very nearly constant up to the highest measuring level on the tower, 30 m. Analysis of balloon data from one day with swell indicates that the layer with constant wind in fact extends to the top of the boundary layer, in this case  $\sim 200$  m. Analysis of the complete swell dataset from the 45 days of the 2003 Baltic Swell experiment shows that the results concerning wind profile shape obtained from the selected cases are generally valid in this experiment. Analysis of the nondimensional wind profile  $\phi_m$  shows that Monin–Obukhov scaling is not valid during swell. Wind and turbulence characteristics are found not to vary to a significant degree with the wind/swell angle within the range of angles encountered,  $\pm 90^\circ$ .

### 1. Introduction

In a broad sense, swell is surface waves traveling faster than the wind. Hristov et al. (2003) have convincingly demonstrated that the airflow above growing waves has the structure predicted by the critical-layer theory of Miles (1957) in actual marine conditions. The essence of this theory is that the depth of the atmospheric layer  $z_c$ , directly influenced by the surface waves with phase speed  $c$ , follows from the relation  $U(z_c) = c$ , where  $U$  is wind speed.

The theory does not explain the interaction between the airflow and swell, but it suggests that the impact of swell waves is likely to extend to an appreciable height, possibly including the entire atmospheric boundary layer. Both theory and actual measurements related to the effect of swell on the atmospheric boundary layer are, however, scarce and fragmentary. This fact may be crucial to parameterization of air–sea interaction in climate models. It is true that swell generally is found in relatively light wind conditions when turbulent fluxes of momentum and heat are expected to be relatively low. On the other hand, swell prevails over a very large percentage of the World Ocean, so it cannot be ruled out that even a possible small systematic error in absolute terms (i.e., in

---

*Corresponding author address:* Ann-Sofi Smedman, Villavagen 16, Uppsala, SE-75236, Sweden.  
E-mail: ann-sofi.smedman@met.uu.se

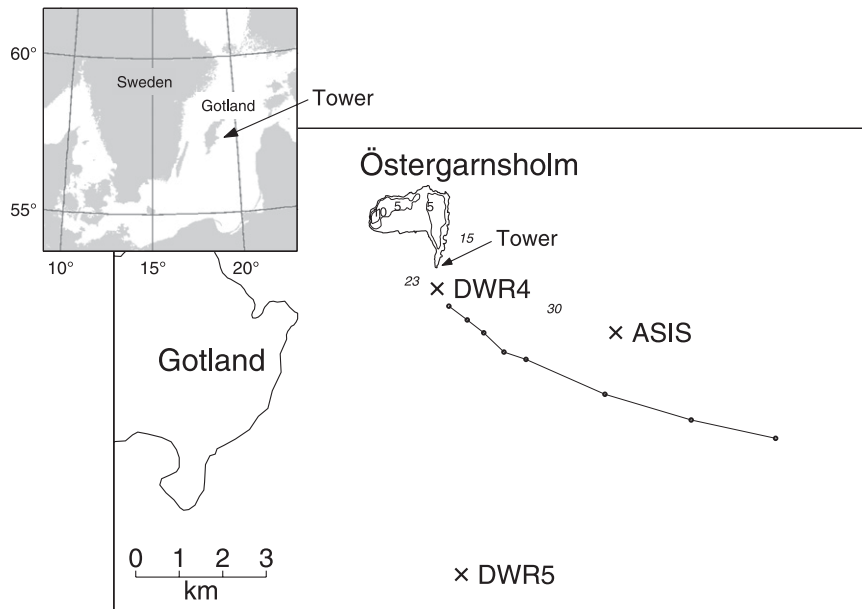


FIG. 1. Map of the BASE area. ASIS, DWR4, and DWR5 are measurement buoys. Anchor depths respectively are ASIS, 36 m; DWR4, 15 m; and DWR5, 43 m. Also shown is a typical measurement track of R/V *Aranda*, conducted 0313–1327 local standard time (LST) 10 Sep 2003. The dots on the track line indicate measurement points. Height contours for 5 and 10 m are shown on Östergarnsholm Island. Numbers in italics are water depths.

$N m^{-2}$  or  $W m^{-2}$ ) might have considerable influence on the outcome of climate simulations, as suggested by Grachev and Fairall (2001).

The first scientific reports of effects from swell on the atmosphere were probably those made during several marine Soviet expeditions in the 1970s (Volkov 1970; Makova 1975; Benilov et al. 1974) and by Davidson and Frank (1973) over Lake Michigan. Studies outside the Australian coast were reported by Antonia and Chambers (1980) and Chambers and Antonia (1981). Later studies include Donelan et al. (1997), Grachev and Fairall (2001), and several papers related to investigations in the Baltic Sea by the Uppsala group: Smedman et al. (1994, 1999), Rutgersson et al. (2001), Sjöblom and Smedman (2002), and Smedman et al. (2003). Laboratory studies with mechanically generated idealized monochromatic waves were reported by Harris (1966), Lai and Shemdin (1971), and Donelan (1987). In a series of papers, Sullivan and coworkers have reported first on direct numerical simulations (DNS) of the effects on the overlaying atmosphere of a fast-moving two-dimensional monochromatic wavy surface (Sullivan et al. 2000) and later on high-resolution large-eddy simulations (LES) of the same problem (Sullivan et al. 2004, 2008). These simulations produce a characteristic low-level wind maximum and other features that are distinctly different from what is found with other boundary

conditions, such as a flat surface or a surface with stationary waves.

The present paper is based on analysis of measurements made in the Baltic Sea within the joint U.S.–Swedish–Finnish Baltic Sea Swell Experiment (BASE), which was conducted at and around the Uppsala University Meteorology Group (MIUU) tower at Östergarnsholm in the Baltic Sea in September–October 2003. The experiment and a detailed study of the homogeneity of the atmospheric conditions in flow from the direction with a long undisturbed over-water fetch is presented in Högström et al. (2008, hereafter H08). The tower was equipped with Solent sonic anemometers at 10, 18, and 26 m and additional slow-response wind and temperature sensors on five levels in the height range 8–30 m above mean water level. The University of Miami group supplied an instrumented Air–Sea Interaction Spar (ASIS) buoy, which was anchored in 36-m-deep water roughly 4 km southeast of the tower, which is upwind of the tower for the range of wind directions considered here (see the map in Fig. 1 as well as section 2 for instrumental details). The Finnish Institute of Marine Research supplied two directional Waverider buoys and carried out a series of cruises with the research vessel R/V *Aranda* (example of track in Fig. 1). A series of radio soundings were conducted at Östergarnsholm and onboard *Aranda*.

As further outlined in section 2, the ASIS buoy was equipped with sonic anemometers at two levels, 2.56 and 5.3 m above the water surface, so that turbulence measurements were made simultaneously at five levels in the height range 2.56 to 26 m above the water surface. Slow-response profile data were recorded at two levels on the buoy, 1.18 and 2.44 m and, as already noted, at five levels between 8 and 30 m on the tower. This means that we have access to very detailed profiles of mean wind and turbulence characteristics in the lowest 30 m of the atmosphere during swell conditions. In addition, the radio soundings gave additional information up to heights well above the boundary layer.

The present paper is a phenomenological treatment of data during swell conditions. Section 2 gives instrumental details and describes criteria for selection of data. Section 3 presents the results and section 4 contains a discussion and conclusions. In a companion paper, Högström et al. (2009), the mechanism that creates the situation presented in the present paper is discussed.

## 2. Instrumentation and data selection criteria

### a. Instrumentation

Here only a brief summary of the instrumentation during the BASE experiment is given. For a detailed description, see H08.

The Östergarnsholm tower is situated on the southernmost tip of the island of Östergarnsholm (Fig. 1), with the tower base 1.3 m above mean sea level (which varied by  $\pm 0.2$  m during the experiment). Unobstructed long ( $>100$  km) over-water fetch occurs for tower wind measurements in the range  $80^\circ < \phi < 210^\circ$ . Solent 1012 sonic anemometers are mounted at 9, 16.5, and 25 m above the tower base. Slow-response (profile) sensors for temperature (copper–constantan thermocouples in ventilated radiation shields) and wind (light cup anemometers and vanes of in-house design) are mounted at 6.9, 11.8, 14.3, 20.2, and 28.8 m above the tower base. In the text we will use nominal mean heights above sea level: 10, 18, and 26 m for the turbulence instruments and 8, 13, 16, 22, and 30 m for the profile instruments. Both turbulence and profile data are 30-min averages. The general procedure for the turbulence data was to remove a linear trend for each 30-min block before calculating turbulent deviations. For calculation of 30-min means for Reynolds stress and the variances of the velocity components, a spectral method described in section 2d was employed instead.

The ASIS (see Fig. 2 in H08) is an anchored multiple-spar buoy, which can be described as a pentagonal cage of slender cylinders (Graber et al. 2000). Most of the

spar buoy is immersed into the water, with only  $\sim 100$  cm of the cylinders extending into the air. On top of the cylinders, there is an open platform that is the base of a slender 4.5-m-long open lattice mast with triangular sections and 0.15-m sides. The meteorological instrumentation on ASIS consisted of (i) two Gill R2A sonic anemometers at 2.56 and 5.3 m above mean sea level; (ii) air temperature and humidity at 4.3 m (shielded Vaisala HMP sensor); (iii) mean wind speed and direction, using Vaisala WM301 cup anemometers and vanes at 1.18 and 2.42 m; and (iv) air temperature using ventilated copper–constantan thermocouples at 0.7 and 1.7 m above mean water level. An array of capacitance wave gauges were used to measure surface elevation and directional spectra, following Pettersson et al. (2003). Both the sonic anemometers and the wave gauges were corrected for the motion of the ASIS, which was measured with a motion package as described in some detail in H08. Further instrumentation on ASIS included thermistors for measuring sea surface temperature. The current profile was obtained from an upward-looking acoustic Doppler current profiler (ADCP) moored near ASIS.

Directional wave parameters were also measured with two Datawell directional Waverider buoys at the positions denoted DWR4 and DWR5 in Fig. 1, moored respectively in 15-m-deep (DWR4) and 43-m-deep water (DWR5).

ASIS, the tower, and the Waveriders were operated simultaneously and continuously during the time period 3 September–10 October 2003. All data were averaged over 30-min periods, and a fully synchronous dataset was established (see next subsection).

R/V *Aranda* (seen in Fig. 2 in H08) made two cruises during the experiment, one in the beginning and one at the end, with the total measuring period being approximately 7 days. Turbulence measurements were performed with a sonic anemometer on a mast in the bow, ship motions being removed from the signals with the aid of a motion package. Measurements were performed along several tracks in the vicinity of ASIS and the tower, similar to the one shown as an example in Fig. 1.

### b. General characteristics of the BASE dataset

As outlined in H08, a dataset for BASE that fulfills basic criteria in terms of wind direction and data completeness includes 750 half-hour values. This dataset formed the basis of an analysis of the properties of the data in general and of the uniformity of the atmospheric regime in the area in particular. Note, however, that the H08 study did not include cases with swell.

It was clearly demonstrated that in the mean, the same momentum fluxes are measured on the tower and on ASIS. A similar result is obtained for the flux of sensible

TABLE 1. Overview of bulk characteristics for the five swell cases C1, C2, C3, F1, and F2, where  $C$  stands for cross swell and  $F$  for following swell, and one reference growing sea case, Grsea. The ‘‘Sullivan’’ case is from LES by Sullivan et al. (2004, 2008). In the top row,  $N$  is the number of half-hour data points that compose each case;  $U_{20}$  = mean wind speed at 20 m;  $u_{*2.5}$  = friction velocity derived from turbulence data at 2.56 m;  $L_{2.5}$  is the Obukhov length, calculated from 2.56 m data;  $\phi_{2.5}$  = wind direction at 2.56 m;  $\phi_d$  = swell direction;  $\Delta\phi = \phi_{2.5} - \phi_d$ ;  $(f_p)_d$  = peak frequency for swell in the wave spectrum (or, for the growing sea case, the peak frequency);  $H_s$  = significant wave height;  $\lambda_d$  = representative wavelength; w.s. = wave slope =  $ak$ , where  $a$  = wave amplitude and  $k = 2\pi/\lambda_d$  = wavenumber (we approximate  $a \approx 0.36H_s$ ); and  $c_p/U_8$  = wave age.

Case	$N$	$U_{20}$ (m s <sup>-1</sup> )	$u_{*2.5}$ (m s <sup>-1</sup> )	$10^3 w' \theta'_v$ (m s <sup>-1</sup> K)	$L_{2.5}$ (m)	$\phi_{2.5}$ (°)	$\phi_d$ (°)	$\Delta\phi$ (°)	$(f_p)_d$ (Hz)	$H_s$ (m)	$\lambda$ (m)	w.s.	$c_p/U_8$
C1	10	1.36	0.00	1.7	0	184	79	105	0.24	0.32	28	0.026	4.72
F1	5	1.45	0.00	1.7	0	153	158	-5	0.22	0.30	33	0.021	4.60
C2	12	3.99	0.095	9.6	-6	160	40	120	0.22	0.22	33	0.015	1.79
C3	19	4.51	0.137	5.1	-37	175	50	125	0.22	0.22	33	0.015	1.61
F2	12	5.51	0.158	20.9	-23	200	190	10	0.17	0.60	47	0.029	1.73
Grsea	10	5.6	0.17	35	-43	148	—	—	0.42	0.26	8	0.07	0.63
Sullivan	—	5.0*	—	10	—	—	—	0	—	4.5	100	0.1	2.5

\* Geostrophic wind speed.

heat, but because the flux was often close to the detection level, scatter was much more prominent than for the case of the momentum flux. This result thus clearly indicates uniformity of the turbulent characteristics of the airflow with wind coming from the sector with long over-water fetch. This conclusion was further substantiated by analysis of the turbulence data from the measurements during the transects with R/V *Aranda*. This finding is fundamental for the analysis presented in the present paper, in which data from the tower and ASIS are combined into a unified analysis covering the entire atmospheric column from 2.5 to 30 m.

A puzzling result of H08 was obtained in the case of wind profile analysis for the nonswell cases. As anticipated, it was found that dimensionless wind gradients  $\phi_m(z/L) = kz/u_* \partial U/\partial z$  could be expressed as functions of  $z/L$  for both unstable and stable conditions. Here  $z$  is height above the water surface,  $U(z)$  is mean wind speed, and  $L$  is the Obukhov length,

$$L = -\frac{u_*^3 T_0}{gk w' \theta'_v}, \quad (1)$$

where  $u_* = \sqrt{-u'w'}$ , the friction velocity (m s<sup>-1</sup>),  $T_0$  is the mean temperature of the atmospheric surface layer in Kelvin,  $g$  is acceleration of gravity (m s<sup>-2</sup>),  $k$  is the von Kármán constant = 0.40, and  $w' \theta'_v$  is the vertical flux of virtual potential temperature (m s<sup>-1</sup> K<sup>-1</sup>). Integrating  $\phi_m(z/L)$  for individual profiles (formed over a succession of 30-min values) gives a good fit to observed wind values for an ASIS layer and a tower layer separately, but extrapolation of the ASIS profile to the lowest tower level, 8 m, gives values that deviate typically by  $\pm 0.5$  m s<sup>-1</sup> from the corresponding measured values on the tower. These deviations were, however, found to be completely random, and in the mean, agreement between measured

values and integrated  $\phi_m$  curves for stable and unstable growing sea conditions was better than 0.1 m s<sup>-1</sup> for all levels from 1.18 m on ASIS to 30 m on the tower. Analysis of the coherence function  $\text{Coh}(n)$  for wind at Östergarnsholm and at ASIS explained the unexpected result. The coherence of the longitudinal wind component at 5 m on ASIS and 10 m on the tower is

$$\text{Coh}(n) = \frac{\text{Co}_{u5,u10}^2(n) + Q_{u5,u10}^2(n)}{nS_{u5}(n)nS_{u10}(n)}, \quad (2)$$

where  $nS_u(n)$  is longitudinal velocity component spectra at 5 m on ASIS and at 10 m on the tower, where  $n$  is frequency (Hz) and  $\text{Co}_{u5,u10}(n)$  and  $Q_{u5,u10}(n)$  are co-spectra and quadrature spectra based on the longitudinal wind data from ASIS (5 m) and the tower (10 m), respectively.

For the conditions reported in H08, which are typical for nonswell unstable and stable conditions with mean wind speed around 10 m s<sup>-1</sup>, the wavelength  $\lambda$  corresponding to  $\text{Coh} = 0$  was found to be about 6 km; for  $\text{Coh} = 0.5$ ,  $\lambda = 30$  km and for  $\text{Coh} = 1.0$ ,  $\lambda = 60$  km. This was interpreted as effects of longitudinal streaks in the surface layer. As demonstrated in section 3a, the situation is radically different for cases with swell, with corresponding  $\lambda$  values being much smaller.

### c. Selection of data for the swell study

Out of the basic dataset of 750 values, 147 half-hour values have  $c_p/U_8 > 1.2$ , where  $c_p$  is peak wave phase speed and  $U_8$  = mean wind speed at 8 m, and unstable stratification, defined as positive heat flux, is  $w' \theta'_v > 0$ . Note our choice of  $c_p/U_8$  for wave age. Sometimes the cosine of the relative wind angle is included; for reasons explained in the appendix, we choose not to include this factor. This is the pool of swell data out of which five cases were selected

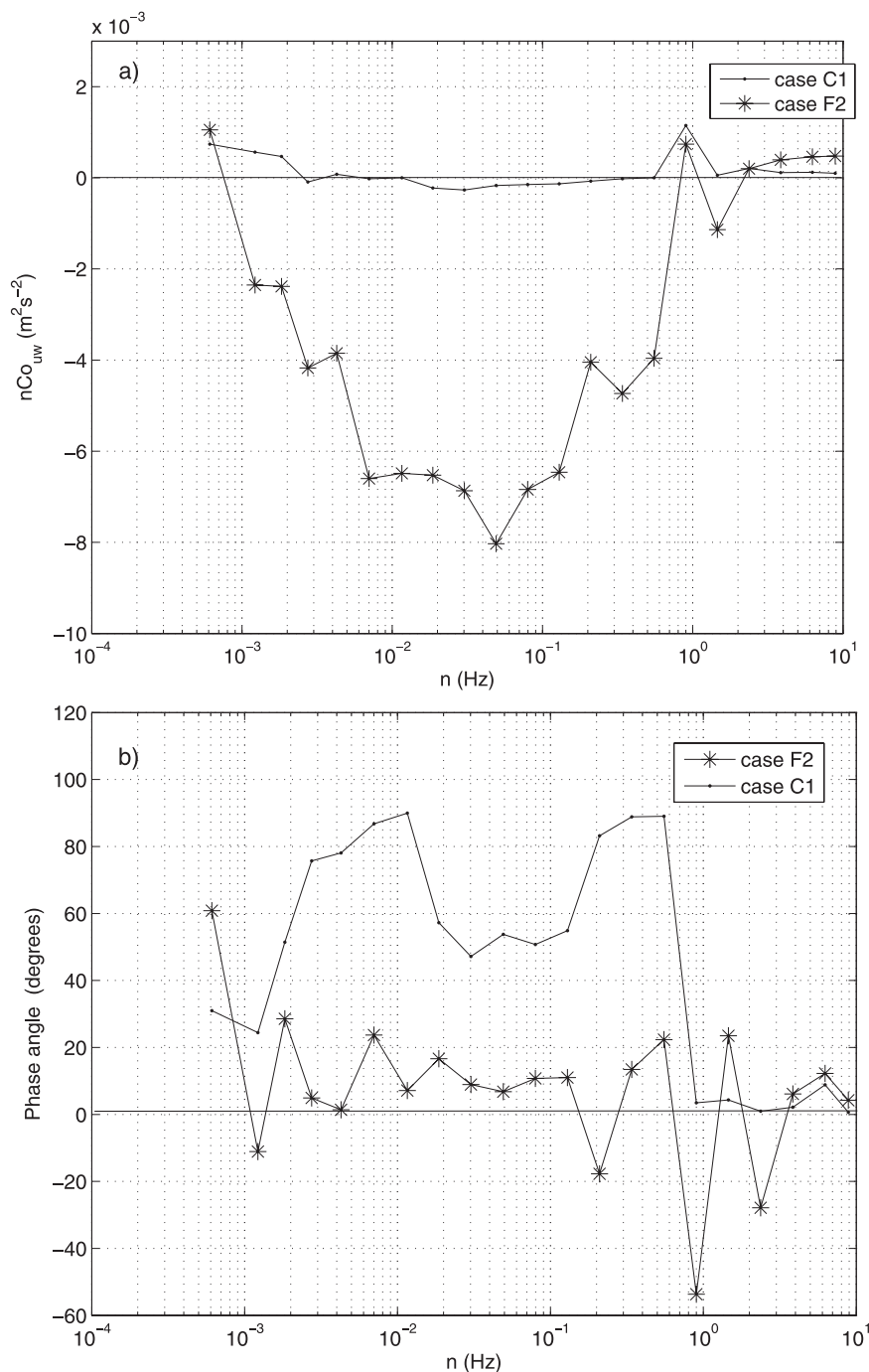


FIG. 2. Examples of (a)  $u-w$  cospectra and (b) phase angles from  $z = 2.56$  m for one case with near-zero  $u'w'$  (C1) and one case with  $u'w' < 0$  (F2).

for the present study. In addition to the criteria defined above, the following criteria were enforced:

- (i) A further data quality check was made, so that values when the wind was coming from behind the sonic anemometers on ASIS (which sometimes

happened in light wind conditions) were removed; in addition, a few data with clearly excessive third-order moments were removed.

- (ii) Periods with several hours of reasonably uniform conditions were required for each case. Thus, each case consists of 5–19 half-hour periods, and all

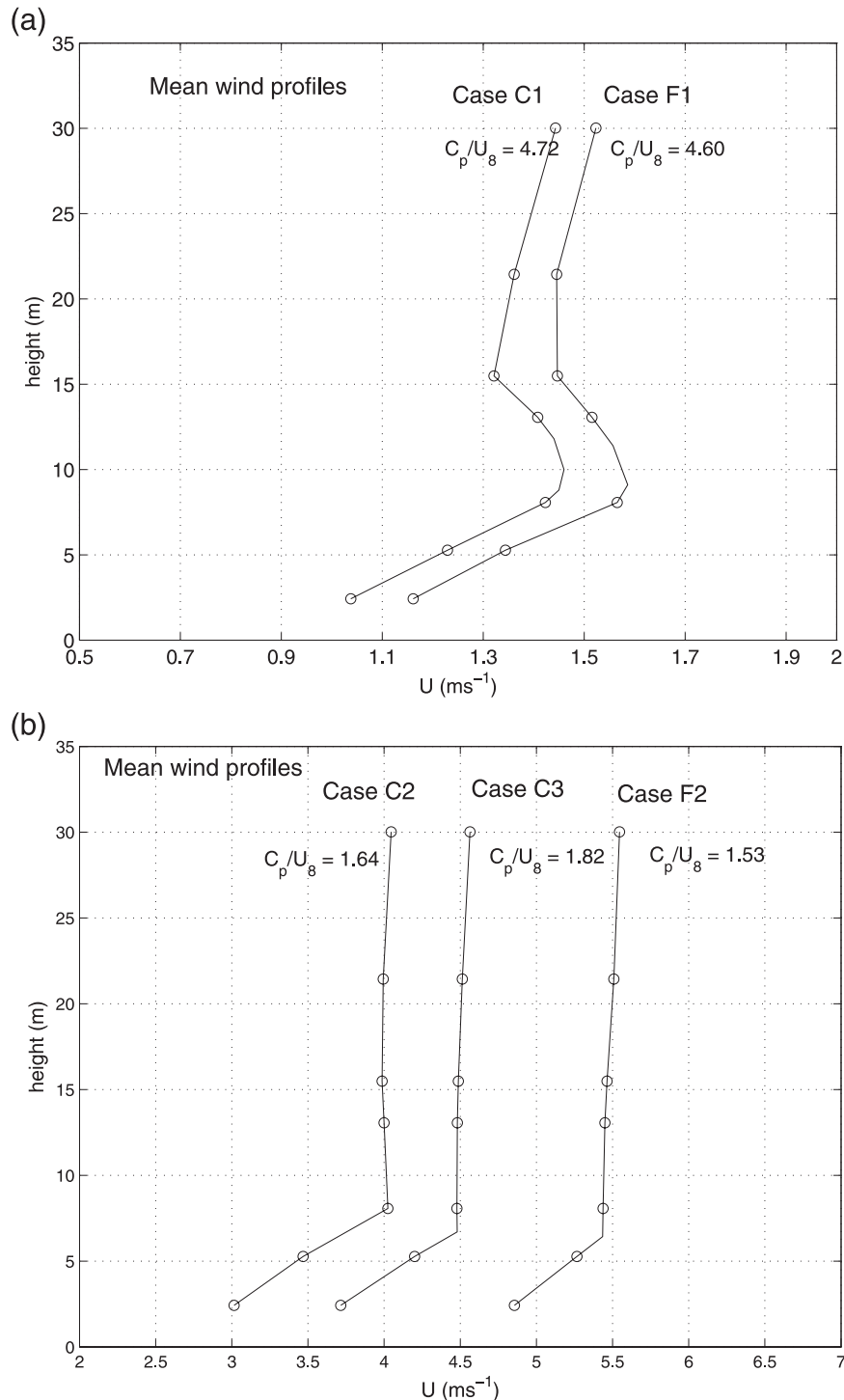


FIG. 3. Mean wind profiles for cases (a) C1 and F1 and (b) C2, C3, and F2.

quantities studied are mean values for each particular case period. This procedure was adopted to ensure reasonable stationarity and to reduce scatter. Two of the cases (C1 and F2; see below) are

made up of two separate cases, each consisting of 5–6 successive half-hour periods).

(iii) Two cases for relatively high wave age ( $c_p/U_8 > 4$ ) and three with  $1.5 < c_p/U_8 < 1.8$  were selected.

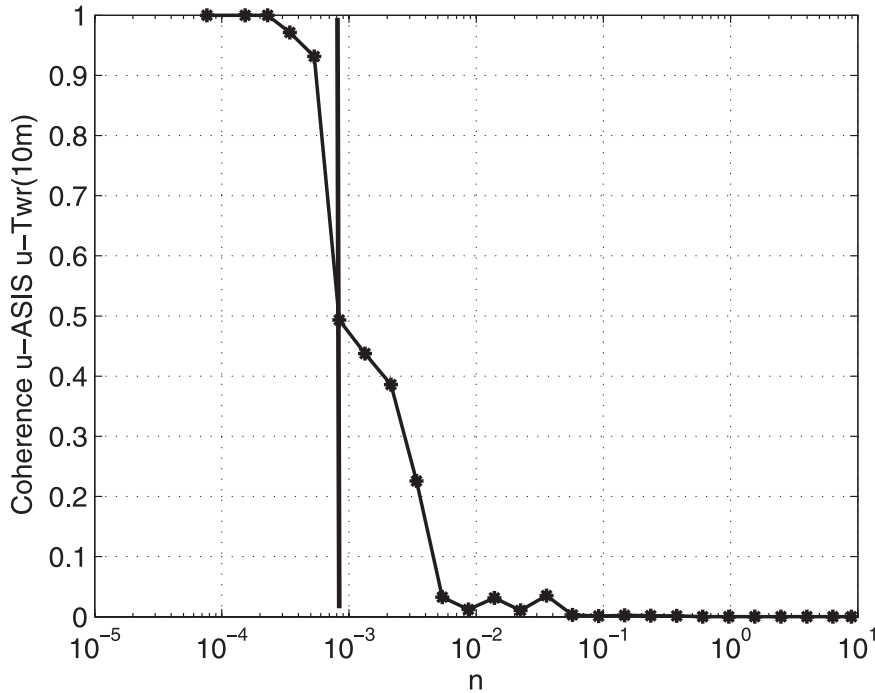


FIG. 4. Coherence of wind at 5 m, ASIS, and 10 m on the tower, on a linear scale, plotted against frequency  $n$  on a logarithmic scale. Data are from a 4-h period with  $c_p/U_8 = 2.1$  and  $U_8 = 3.5 \text{ m s}^{-1}$ , starting at 0830 LST 6 Sep 2003.

Table 1 gives an overview of relevant data for the five selected swell cases. For comparison, data were also evaluated for a case (denoted Grsea in Table 1) with growing sea conditions,  $c_p/U_8 = 0.63$ , which has wind speed at 20 m similar to that of swell case F2,  $U_{20} = 5.6 \text{ m s}^{-1}$  and similar  $L = -43 \text{ m}$ . It is based on the mean of 10 consecutive half-hour periods. The last line gives data for the “fast wave, weak wind, unstable” large-eddy simulation of Sullivan et al. (2004, 2008).

The wave field in cases with swell was approximated by a single swell component coming from a certain direction (see the column denoted  $\phi_d$  in Table 1), combined with shorter waves caused by the local wind and traveling in the direction of the wind ( $\phi_{2.5}$  in the table). The mean angle  $|\Delta\phi|$  between the direction of the dominating swell waves and the wind varied considerably. Thus, two groups of cases were selected: (i) following-swell cases, including cases in which  $|\phi_d - \phi_{2.5}| < 10^\circ$ , cases F1 and F2, and (ii) cross-swell cases, in which  $|\phi_d - \phi_{2.5}| \approx 90^\circ$ , cases C1, C2, and C3. Cases C2 and C3 have swell that comes from direction  $40^\circ\text{--}50^\circ$ . For this direction, the wave field at wave buoy DWR4 is likely to be distorted because of a shoaling area east of Östergarnsholm (H08). However, no influence is expected at ASIS and DWR5. The measurements on the tower ( $8 \text{ m} < z < 30 \text{ m}$ ) may be expected to suffer some distortion if the flux footprint lies over the distorted wave

field, but analysis (not shown) fails to show any significant sign of this.

*d. Evaluation of shearing stress and wind component variances*

Under nonswell conditions, it is in most cases straightforward to evaluate the shearing stress,  $u'w'$ , from linear plots of the frequency-premultiplied  $u\text{--}w$  cospectrum,  $n\text{Co}_{uw}(n)$ , against frequency  $n$  on a logarithmic scale or from the corresponding ogive curve (i.e., cumulative spectral representation). Deriving stress from cospectra and ogive curves for situations with swell is, however, more complicated. The reason for this is the frequent occurrence of large-amplitude positive and negative excursions in  $n\text{Co}_{uw}(n)$  at relatively low frequencies, typically in the range  $10^{-4} < n < 10^{-2} \text{ Hz}$ , and with large phase angles. A signature of ordinary turbulence in shear flow is a small phase angle between the fluctuations in  $u$  and  $w$ , typically  $< 20^\circ$ . The cospectral variations in this spectral band, which have a large phase angle, are thus not turbulence but random, high-amplitude noise (i.e., mesoscale fluctuations not related to local conditions; cf. Vickers and Mahrt 2003, 2006).

Looking at the phase angle as function of frequency for the five swell cases gives the following results. For the two cases with large wave age values, C1 and F1, the phase angle is in the range  $40^\circ\text{--}90^\circ$  for all frequencies

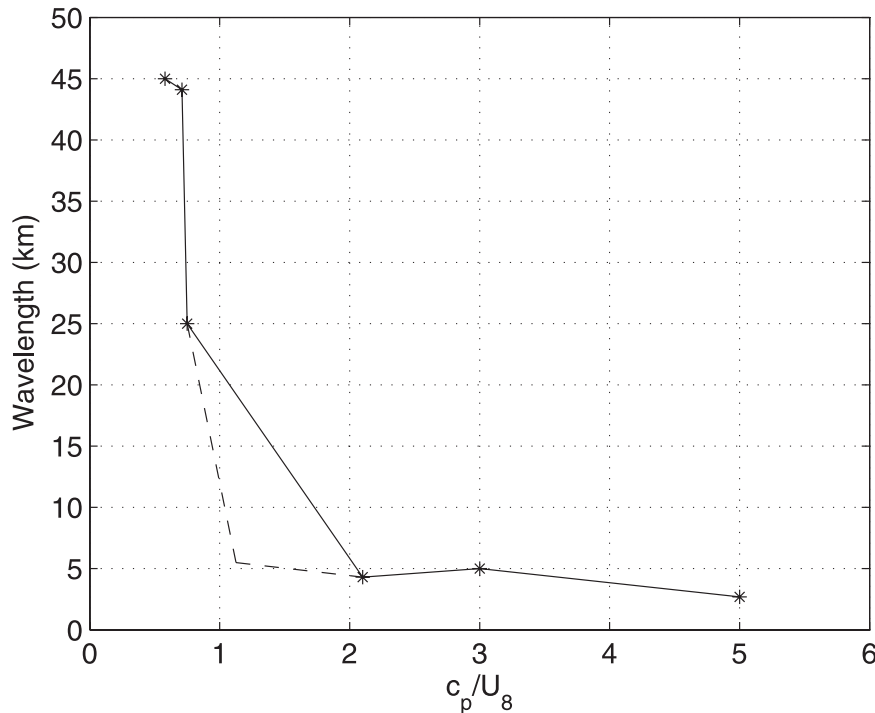


FIG. 5. Wavelength at  $\text{Coh}_{U5U10} = 0.5$  plotted as function of wave age,  $c_p/U_8$ . Stars are measurements, connected by full lines. Dashed lines indicate a possible alternative curve shape for  $0.8 < c_p/U_8 < 2.1$ , assuming a gradual rise with decreasing wave age from the measured value at  $c_p/U_8 = 2.1$  to 1.2, where a sharp rise to the measured value at  $c_p/U_8 = 0.8$  occurs.

and heights. For the remaining three cases, C2, C3, and F2, the phase angle is  $<40^\circ$  for frequencies  $>n_{\min}$ , where  $n_{\min}$  is in the range  $10^{-3}$ – $10^{-2}$  Hz.

As an illustrative example, Fig. 2a shows cospectra for cases C1 and F2 and Fig. 2b shows the corresponding phase angles from the lowest measuring height, 2.56 m. For case C1 the cospectral level is very low and the phase angle is in the range  $40^\circ$ – $80^\circ$ , so we conclude that a “true” value of  $\overline{u'w'}$  cannot with certainty be distinguished from zero. The same conclusion can be drawn from corresponding plots for case F1 (not shown) and for all five measuring heights. For case F2, the phase angle is small for all frequencies  $<10^{-3}$  Hz, and we conclude that a good estimate of  $\overline{u'w'}$  is obtained by integrating the cospectral curve over the frequency range  $10^{-3} < n < 1$  Hz.

For cases C2, C3, and F2 in general (i.e., considering spectra and phase angles from all five heights), the phase angle is in the range  $10^\circ$ – $20^\circ$  for frequencies above  $n_{\min}$ , but for lower frequencies it becomes large. From the shape of the cospectra and ogive curves it is concluded that for these cases 70%–80% of the momentum flux is contained in the frequency band with low phase angles. The remaining 25%–30% is obtained through extrapolation of the cospectral curve to  $n\text{Co}_{uw}(n) = 0$ . This

procedure is admittedly subjective but probably not systematically biased (as an arbitrary choice of a low-frequency cutoff frequency would be). We estimate the random uncertainty of these estimates of  $\overline{u'w'}$  to be about  $\pm 20\%$ .

Variances of the wind components ( $\sigma_u^2$  and  $\sigma_w^2$  for the longitudinal and vertical components, respectively) were evaluated in a similar manner as  $\overline{u'w'}$ ; that is, spectra were plotted and what was considered low-frequency noise was subjectively removed.

### 3. Results

#### a. Wind profiles

Figures 3a and 3b show the mean wind profiles for the five swell cases. Notice that each of these profiles is a composite of an ASIS profile for the layer 2.4–5.3 m and a tower profile for the layer 8–30 m. For cases C1 and F1 in Fig. 3a, the extrapolation from 5 to 8 m is straightforward; for the layer between 8 and 13 m, the exact shape of the curve is not known, although it is clear that there must be a maximum as indicated in the figure. Figure 3b shows the profiles for cases C2, C3, and F2. For each of these profiles, it is obvious that there is a layer

with strong gradient near the surface and a layer of nearly constant wind from somewhere in the range 6–8 m extending to at least 30 m. The exact position of the “knee” that marks the transition from the strong near-surface gradient to  $U = \text{constant}$  is not known; it is possible that the curve has more gentle curvature at the position of the knee. The knee in the three profiles is just an effect of extrapolating the ASIS curve linearly to where it meets the linearly extrapolated “tower curve.”

Although it is not exactly known where the extrapolated ASIS curve and the corresponding tower curve in each case meet, it is clear from the plots in Figs. 3a,b that the possible mismatch is on the order of  $\pm 0.1 \text{ m s}^{-1}$  or less, which is in striking contrast to the profiles for growing sea shown in Fig. 17 of H08, where the mismatch is about  $\pm 0.5 \text{ m s}^{-1}$ . The reason for this can only partly be the much lower wind speeds in the present study compared to the case of the H08 profiles (typically  $10 \text{ m s}^{-1}$ ). A more fundamental cause is found in the scale and organization of the turbulence involved. This can be studied by comparing the coherence function, Eq. (2), for growing sea and for swell as done in H08.

The question was raised by a referee whether the measurements during cases C1 and F1 are really reliable, in view of the very low wind speeds encountered,  $1.1\text{--}1.6 \text{ m s}^{-1}$  (Fig. 3a). It is known from many studies over land that for such cases the wind direction may be quite erratic. However, analysis of the present data clearly shows that wind direction fluctuations during cases C1 and F1 are not excessive. Writing for the total case average standard deviation (std) of direction fluctuations,

$$\sigma_\phi = \sqrt{\sigma_1^2 + \sigma_2^2}, \quad (3)$$

where  $\sigma_1$  is the mean 30-min std and  $\sigma_2$  is the std of the 30-min means, the following mean results are obtained for cases C1 and F1 together as one group and C2, C3, and F2 as another:  $\sigma_1 = 7^\circ$  for the C1, F1 group and  $5^\circ$  for the other group;  $\sigma_2 = 15^\circ$  for the C1, F1 group and  $16^\circ$  for the other group. Thus, the low wind group is very well behaved, showing no erratic fluctuation pattern. Note also that the sonic anemometers used in this experiment were individually calibrated in a big wind tunnel before the experiment and that the instrument responds adequately even at very low wind speeds. As discussed in the companion paper, Höglström et al. (2009), based on analysis of the turbulent kinetic energy (TKE) budget, it is clear that the flow during cases C1 and F1 is completely governed by upward-directed pressure transport of TKE from the swell waves. Thus, these cases represent very well-behaved swell-driven situations, which are particularly apt to comparison with the corresponding LES of Sullivan et al. (2008).

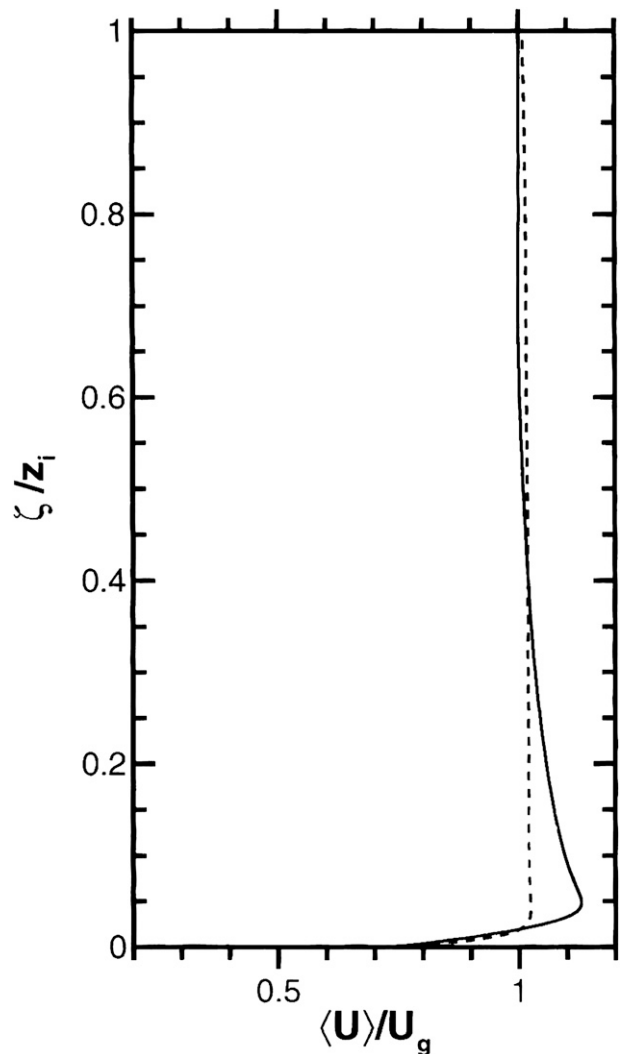


FIG. 6. LES results by Sullivan et al. (2008), showing vertical profiles of the along-wind horizontal component of the normalized mean wind  $\langle U \rangle / U_g$  for flow over waves, where  $U_g$  is the geostrophic wind (assumed height constant). The spatial averaging is carried out along constant  $\zeta$  surfaces, where  $\zeta$  is the mean height above the wave and  $z_i$  is the height of the boundary layer. The figure shows the result for waves traveling with and faster than the wind; the full lines are for strictly neutral conditions and the dashed lines for the case of slight convection. [Adapted from Sullivan et al. (2008).]

Figure 4 shows an example of a coherence plot for a 4-h case with swell,  $c_p / U_g = 2.1$ , and  $U_g = 3.5 \text{ m s}^{-1}$  during BASE. The coherence is close to zero for  $n > 5 \times 10^{-3} \text{ Hz}$ , which corresponds roughly to atmospheric wavelength  $\lambda = U/n \approx 700 \text{ m}$ . Thus, fluctuations on smaller scales than that are completely uncorrelated at ASIS and the tower. For  $n < 2.5 \times 10^{-4} \text{ Hz}$  (i.e.,  $\lambda > 14 \text{ km}$ ), corresponding fluctuations are completely correlated. A value of Coh = 0.5 represents partly correlated fluctuations and

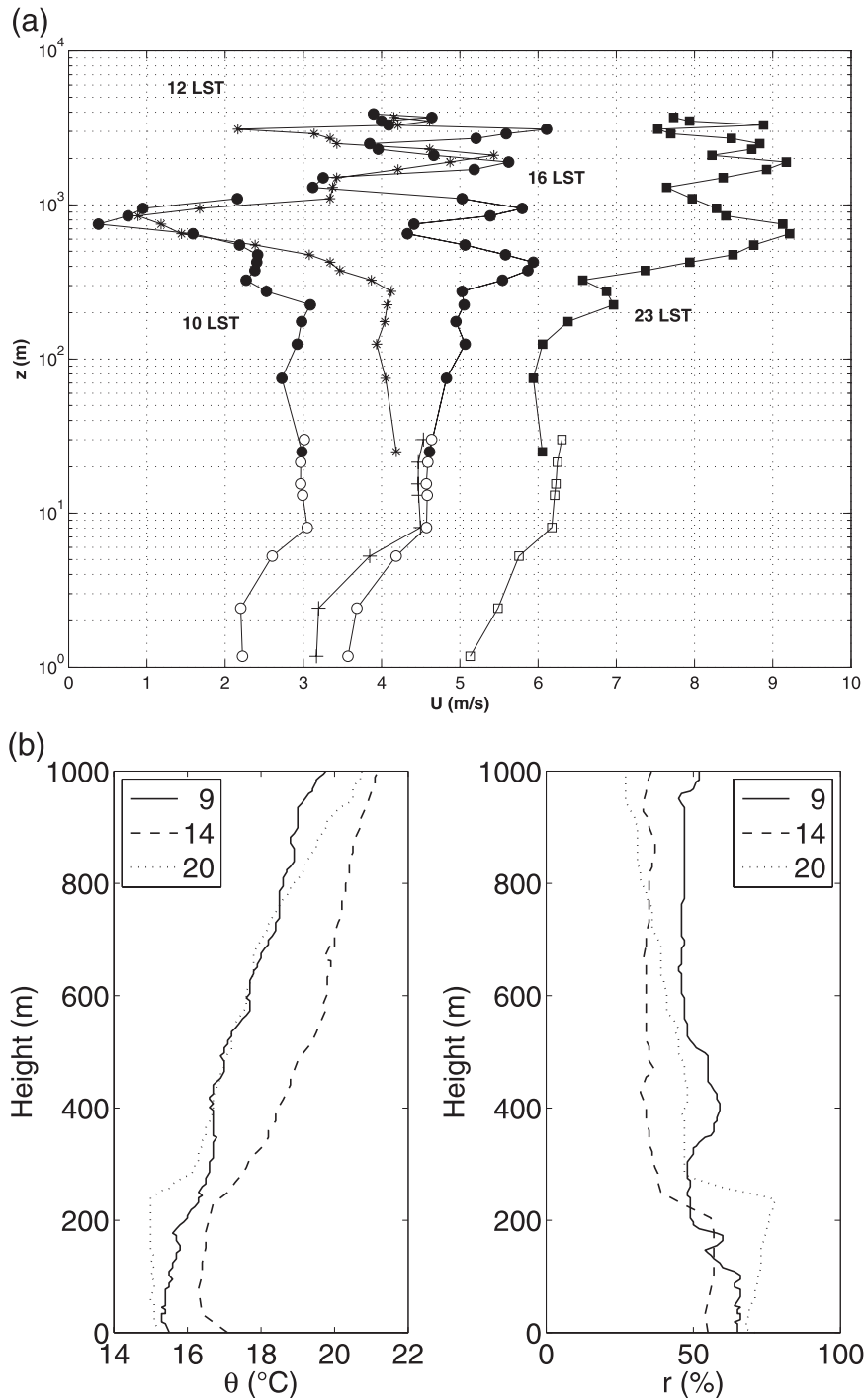


FIG. 7. (a) Results from radio soundings and pilot balloon trackings during one day, 6 Sep 2003. Wind profiles from ASIS and Östergarnsholm tower (open circles, pluses, and open squares) and balloons (filled circles, stars, and filled squares). The height scale is logarithmic; the wind scale is linear. (b) Profiles of potential temperature  $\theta$  and relative humidity  $r$  representative of the period with soundings in (a). Legend figures refer to time in LST.

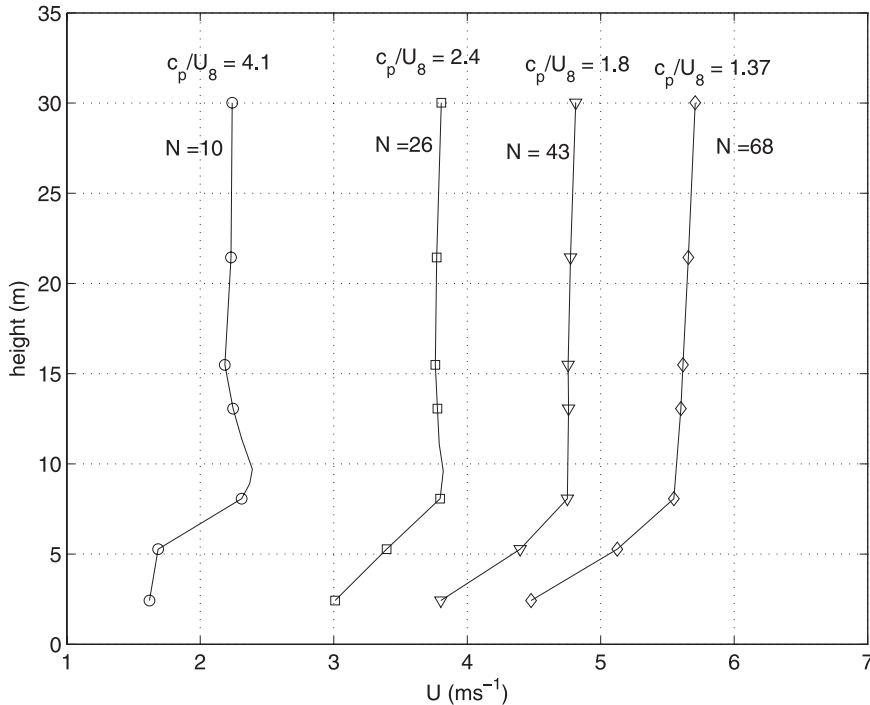


FIG. 8. Mean swell wind profiles, based on the entire BASE dataset. Data have been divided according to wave age,  $c_p/U_8$ , and four mean profiles have been derived;  $N$  = number of half-hour periods in each wave age group. Total number of data = 147.

occurs in this case for  $n_{0.5} = 8 \times 10^{-4}$  Hz (i.e., for  $\lambda_{0.5} \approx 4$  km).

Coherence plots were made for six cases of typically 4–5-h duration, each with different wave age. From each of these,  $n_{0.5}$  was extracted and corresponding  $\lambda_{0.5}$  values were derived. Figure 5 shows  $\lambda_{0.5}$  plotted against  $c_p/U_8$ . For growing sea,  $c_p/U_8 < 0.8$ ,  $\lambda_{0.5}$  is in the range of 25–45 km, but for swell (i.e.,  $c_p/U_8 > 1.2$ ), it is only 2–5 km. This is small compared to the sampling length  $UT$ , where  $U$  is around  $1.5 \text{ m s}^{-1}$  for cases C1 and F1 and  $4\text{--}5 \text{ m s}^{-1}$  for the other three cases and  $T$  is typically  $5 \text{ h} = 1.8 \times 10^4 \text{ s}$ , so that  $UT$  is in the range of 27–80 km.

The reason for the great scale difference between the growing sea cases and the swell cases must lie in the large-scale structure of these two classes of airflow. It is well documented (see H08 for references) that strong-wind near-neutral cases (both slightly unstable and slightly stable) have a turbulence structure near the surface dominated by long streaky structures. For swell, the present coherence analysis thus clearly indicates that characteristic large-scale eddies are an order of magnitude smaller, as also found in the LES of Sullivan et al. (2008; not shown). This feature is advantageous for the present wind profile analysis because it enables drawing reliable profiles from a combination of ASIS and tower data (Figs. 3a,b).

The wind profiles for the five swell cases have either a pronounced low-level wind maximum (cases C1 and F1; Fig. 3a) or a distinct knee (cases C2, C3, and F2; Fig. 3b). This feature is in general agreement with corresponding large-eddy simulations by Sullivan et al. (2008); see Fig. 6, which shows either a pronounced maximum (for the case of following swell) or a knee (for the case of convection with waves traveling with and faster than the wind).

Note also the almost constant wind above the maximum or the knee in the LES. Figure 7a, which combines wind data from ASIS, the tower, and pilot balloon soundings during the course of a day with swell (6 September 2003; case C3 covers the time period between 0900 to 1430 LST; data for the later parts of the day were not included in any of the five selected cases because of slight nonstationarity but are included in the calculation of the mean swell profiles of Fig. 8), shows that this layer of constant wind speed extends all the way up to about 200 m, where drastic wind speed changes occur in each profile. From Fig. 7b it is seen that this height is identical to the height of the boundary layer.

Actual observations of wave-driven wind (i.e., wind profiles with a maximum at a few meters height over water) are scarce in the open literature. Donelan (1990) reproduces a plot from a report by Holland et al. (1981),

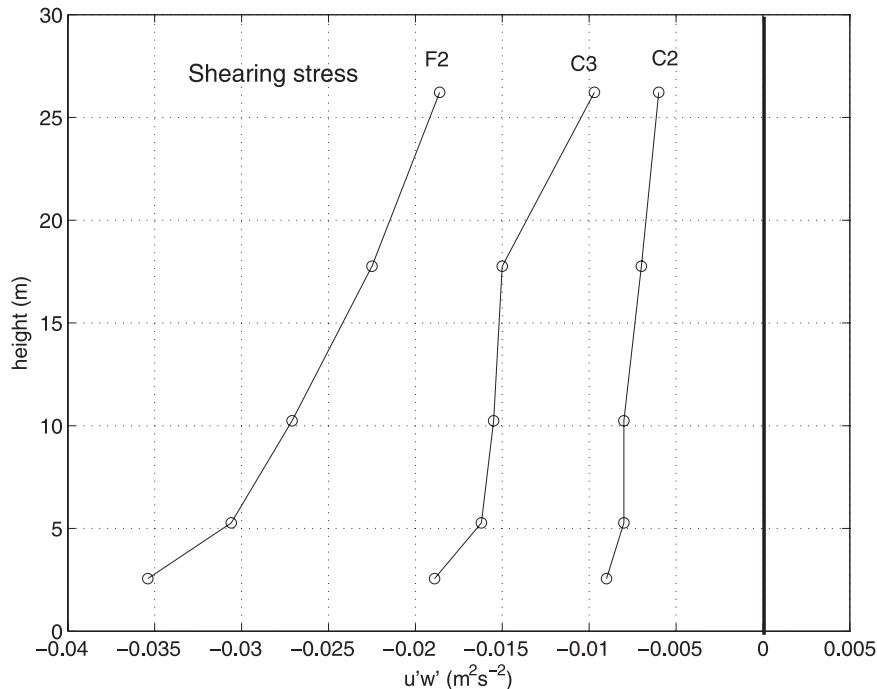


FIG. 9. Mean shearing stress plotted as function of height for cases C2, C3, and F2. For cases C1 and F2,  $u'w'$  is zero at all heights.

which shows the existence of several consecutive profiles with wind maxima in the height range 4–10 m. Smedman et al. (1999) observe persistent negative wind gradients at 10 m (obtained from five cup anemometers in the height range 8–30 m) during a period with persistent swell at Östergarnsholm. Because there were no measurements at that time below 8 m, the actual wind maximum was not observed (but was inferred because of the no-slip requirement at the surface).

It is worth noting the close resemblance in wind profile shape for cases C1 and F1 (Fig. 3a). These cases have roughly the same  $c_p/U_8$  value (4.7 and 4.6, respectively) but drastically different wind/swell angles:  $|\phi_d - \phi_{2.5}| < 10^\circ$  for case F1 and  $105^\circ$  for case C1. Also, cases C2, C3, and F2 (Fig. 3b), with similar  $c_p/U_8$  value (in the range 1.6–1.8) but with  $|\phi_d - \phi_{2.5}| < 10^\circ$  for case F2 and values of around  $90^\circ$  for C2 and C3, have wind profiles of strikingly similar shape. As demonstrated in the text to follow, this apparent insensitivity to the wind/swell angle is found in all studied parameters. An interpretation of this robustness is discussed in the appendix.

The five cases selected for the main analysis of this study have been chosen to represent well-defined conditions in terms of wave age and wind–wave angle, as explained in section 2c. But they are just five samples, each representing a mean over 2.5 to 6 h, so it is relevant to ask: how representative are they of the swell regime during the BASE experiment? In all there are 147 half-

hour periods with swell left after data quality screening. This dataset was divided into four groups according to  $c_p/U_8$ : (i)  $c_p/U_8 > 3$  (mean = 4.1;  $N = 10$ ); (ii)  $2 < c_p/U_8 < 3$  (mean = 2.4;  $N = 26$ ); (iii)  $1.6 < c_p/U_8 < 2$  (mean = 1.8;  $N = 43$ ); and (iv)  $1.2 < c_p/U_8 < 1.6$  (mean = 1.37;  $N = 68$ ). The corresponding mean wind profiles are plotted in Fig. 8. Note that the profiles in Fig. 8 have not been screened for wind–wave angle and that we expect to find some “smearing” when averaging is done. In view of this, the similarity of these profiles with the profiles shown in Figs. 3a,b for similar values of  $c_p/U_8$  is striking.

#### b. Profiles of second-order moments and the $u$ – $w$ correlation

Figure 9 shows profiles of the mean vertical momentum flux for cases C2, C3, and F2. For cases C1 and F1  $u'w'$  is zero at all heights. All fluxes are negative (downward) and decrease in magnitude with increasing height. In their LES, Sullivan et al. (2008) find the momentum flux to be positive (upward) from the surface and throughout the boundary layer for following swell. Positive values of  $u'w'$  have been observed by Grachev and Fairall (2001) and by Smedman et al. (1994), who combined tower measurements and airborne measurements and found  $u'w'$  to be consistently positive in the lowest 100–200 m of the marine atmosphere for a period of about 5 h.

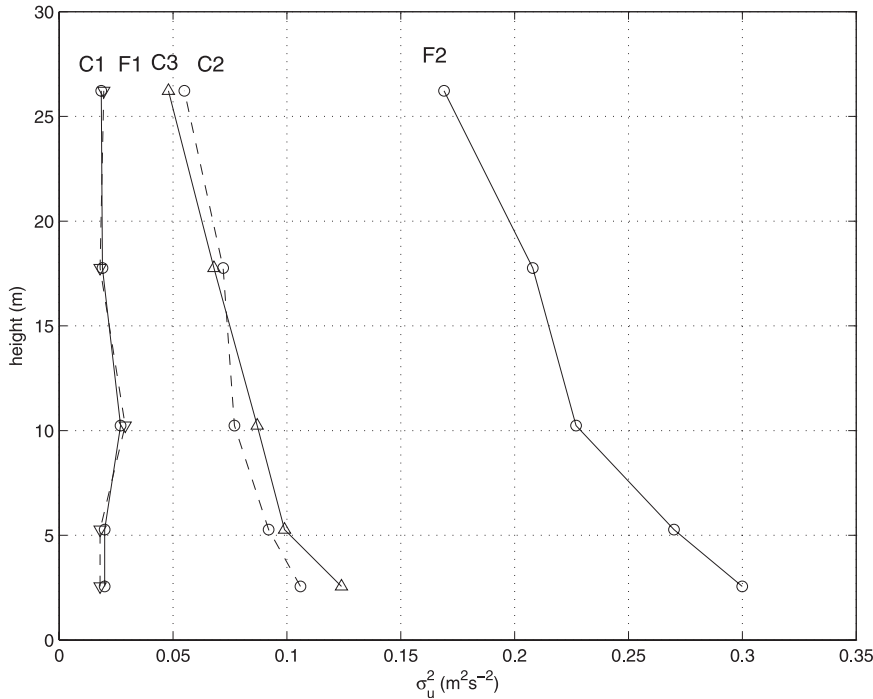


FIG. 10. Mean variance of longitudinal wind fluctuations plotted against height for each of the five swell cases.

Figures 10 and 11 show profiles of  $\sigma_u^2$  and  $\sigma_w^2$ , respectively. Sullivan et al. (2008, their Fig. 13) present the same quantities normalized with the square of the geostrophic wind. Comparisons with our data show that  $\sigma_u^2$  is in qualitative agreement with their curves for “slight convection with waves traveling with and faster than the wind” (not shown);  $\sigma_u^2$  decreases rapidly with height and  $\sigma_w^2$  increases with height, changing the ratio  $\sigma_u^2/\sigma_w^2$  from a value around 5 near the surface to near unity at 30 m in the case of C1 and to about 2.5 for F1, thus indicating a tendency toward local isotropy with increasing height for these high-wave age cases. This is in qualitative agreement with the LES for the dimensionless approximate height range 0.05 to 0.4. Below dimensionless height 0.05, LES shows decreasing  $\sigma_w^2$  with height whereas in our data  $\sigma_w^2$  is increasing all the way. Our interpretation is that this difference results from the swell that induces large wave coherent velocities near the surface. In Sullivan’s LES, the swell is an order of magnitude higher and several times steeper than in our data.

The corresponding profiles for the dimensionless quantities of the remaining swell cases do not differ to a considerable degree from each other.

Figure 12 shows profiles of the  $u$ – $w$  correlation, defined as

$$r_{uw} = \frac{\overline{u'w'}}{\sigma_u \sigma_w}. \quad (4)$$

Cases C2, C3, and F2 have  $r_{uw}$  values in the range  $-0.15$  to  $-0.3$ , and zero for the high-wave age cases C1 and F1. This result is in agreement with the findings in Smedman et al. (1999, their Fig. 7), which gives  $r_{uw}$  as a function of  $c_p/U_{10}$ . It shows, for both the 10-m level and the 26-m level, that  $-r_{uw}$  decreases distinctly from values between 0.3 to 0.4 for  $c_p/U_{10} < 1.2$  to values around 0.2 for  $1.2 < c_p/U_{10} < 2$  and to values in the range 0 to 0.1 for still higher wave age values.

In Smedman et al. (1999) it was noted that strong reduction of  $\overline{u'w'}$  with increasing wave age combined with a relatively high level of fluctuation in the  $u$  and  $w$  components caused the observed reduction of  $-r_{uw}$ . It was argued that “inactive turbulence,” which is brought down from a high-wind shear layer at the top of the boundary layer to layers near the surface by the pressure transport term, was likely to be responsible for the observed reduction of  $-r_{uw}$ . In the companion paper, Höglström et al. (2009), an alternative explanation is presented: the pressure transport term is still considered to play a crucial role, but the source is placed at the surface instead, with the form drag of the swell waves being the most likely mechanism.

#### c. Validity of Monin–Obukhov similarity during swell

It is usually assumed that Monin–Obukhov (MO) theory is valid in the marine surface layer. This would

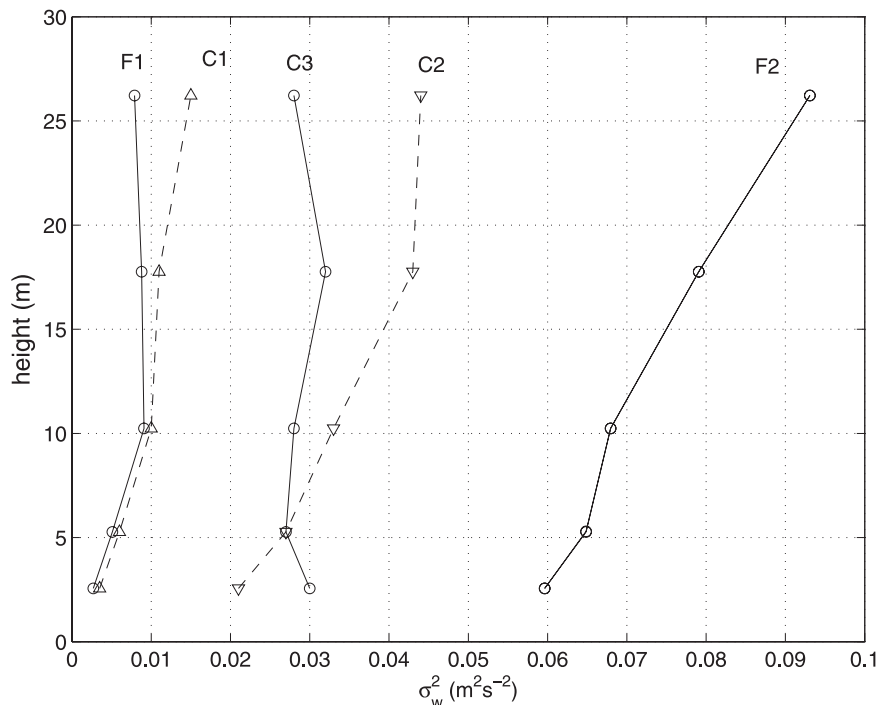


FIG. 11. As in Fig. 10, but for mean variance of vertical velocity fluctuations.

imply that the dimensionless wind gradient  $\phi_m(z/L) = kz/u_* \partial U/\partial z$  could be expressed as functions of  $z/L$ . Over land, the following expression describes well (Högström 1996) the relation during unstable and neutral conditions:

$$\phi_m = (1 - 15z/L)^{-1/4}. \quad (5)$$

In Table 2,  $\phi_m$  (derived in this way for the three lowest measuring heights) is given in the respective columns labeled  $\phi_{m2.56}$  [Eq. (5)],  $\phi_{m5}$  [Eq. (5)], and  $\phi_{m10}$  [Eq. (5)]. The corresponding columns, denoted  $\phi_{m2.56}$  (meas.), etc., have been obtained from the actual measurements of the local wind gradient and friction velocity. It is clear that  $\phi_m$  at 2.56 and 5.3 m is considerably larger than the values obtained for the ideal nonswell case. For cases C2, C3, and F2,  $\phi_m \approx 0$  from 10 to 30 m; for cases C1 and F1, the values are infinite below the height of the wind maximum and indeterminate at the wind maximum itself (because both  $u_*$  and  $\partial U/\partial z$  are zero). In the height range 8–15 m,  $\phi_m$  is  $-\infty$ ; at around 15 m there is a local minimum in the wind profile, implying that  $\phi_m$  is indeterminate at that particular height; above 15 m it is  $+\infty$  because the wind gradient is finite but the friction velocity is zero. From this it can be concluded that MO theory is not valid at any height for any of the five swell cases studied here; expressed in other words, there is no unique relation between the local wind gradient and the momentum flux. As discussed in detail in the companion paper, Högström

et al. (2009), this feature is due to the combined effect of wave-induced upward momentum transport from the swell waves and ordinary downward turbulent transport in the opposite direction caused by shorter (and hence slower) waves traveling on top of the swell waves. In Högström et al. (2009) it is further shown that the two high-wave age cases C1 and F1 are completely dominated by the swell-induced effect.

#### 4. Summary and conclusions

Analysis of the wind profiles for the five selected cases with swell shows a persistent pattern, which is remarkably independent of wind swell direction, at least for  $|\phi_d - \phi_{2.5}| \leq \sim 90^\circ$ . The cases with relatively large wave age,  $c_p/U_8 > 4$  (C1 and F1), experience a clear wind maximum slightly below 10-m height, whereas the remaining cases (C2, C3, and F2), for which  $2 > c_p/U_8 > 1.5$ , all have a characteristic knee in the wind profile in the height range 6–8 m, meaning that the wind increases rapidly with height below the knee, being close to constant with height above that point. These features are not specific for the five selected cases but show up equally distinctly in an analysis of all the cases with swell during the nearly 2-month duration of the BASE experiment (147 half-hour values). An example from a day with prevailing swell conditions when wind profiles were obtained from balloon measurements up to several kilometers on four occasions (Fig. 7) indicates that the wind

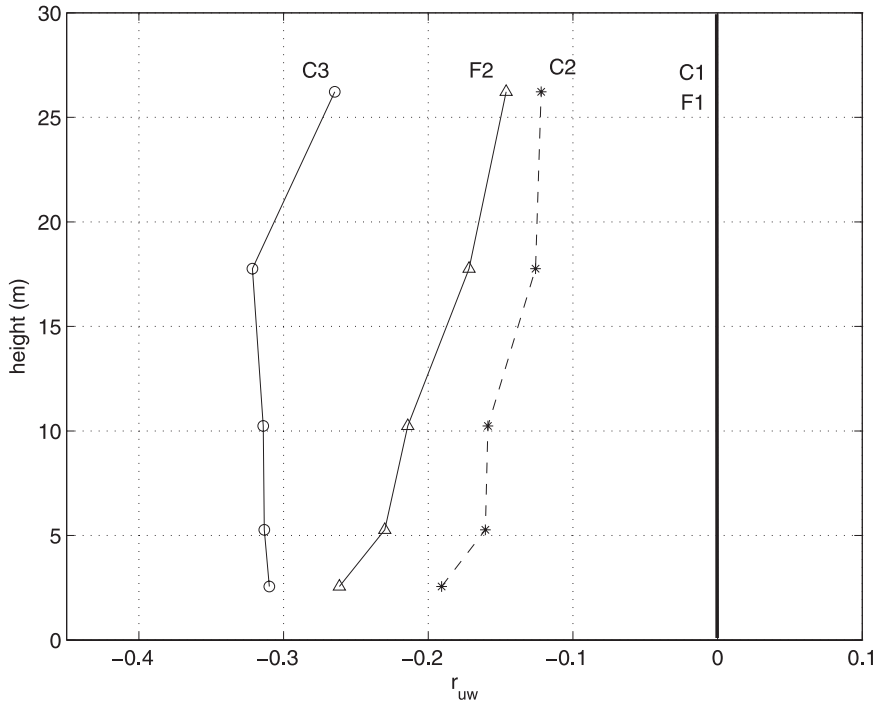


FIG. 12. Profiles of the correlation coefficient  $r_{uw} = \overline{u'w'}/\sigma_u\sigma_w$  for the five swell cases. Note that for cases C1 and F1,  $r_{uw} = 0$ .

was essentially height constant throughout the entire boundary layer, in this case about 200 m. The findings from the wind profile study are in general agreement with the LES results of Sullivan et al. (2008), who find from their large-eddy simulations that the swell-induced atmospheric signatures are global. Our results are also in broad agreement with the findings of Hanley and Belcher (2008) obtained with a simple 1D model.

The shearing stress is either zero at all heights (cases C1 and F1) or negative at all heights, the magnitude decreasing with height. The LES of Sullivan et al. (2008) and the 1D model of Hanley and Belcher (2008) give slightly positive shearing stress for the wind-following swell case. Such results have been found earlier in atmospheric studies by Smedman et al. (1994) and Grachev and Fairall (2001). As shown in Högström et al. (2009), the shearing stress during swell is the sum of a positive term, induced by the swell component and a negative

term, which is due to the effect of the shorter waves. The sign of the net stress thus depends on the relative magnitude of the two terms.

The turbulence structure of the swell boundary layer was further studied by plotting profiles of variances of the longitudinal and vertical wind components. The shape of the variance profiles were found to vary strongly with wave age. Profiles of the  $u-w$  correlation show  $-r_{uw}$  to be smaller than expected for corresponding nonswell cases.

An analysis of the dimensionless wind gradient  $\phi_m$  demonstrated that Monin–Obukhov theory is not valid during swell. Thus, instead of a steady decrease with height from a value of unity at the surface expected for an unstable atmospheric surface layer,  $\phi_m$  values much in excess of unity are found for 2.56 and 5.3 m, contrasting strongly with the conditions above the maximum or the knee around 10 m, where  $\phi_m$  is close to zero. Because Fig. 7 shows the wind to be constant up to the top of the

TABLE 2. Dimensionless wind gradient  $\phi_m$  for 2.56, 5.3, and 10 m, estimated from the measurements (“meas.”) and from Eq. (5), respectively.

Case	$\phi_{m2.56}$ (meas.)	$\phi_{m2.56}$ [Eq. (5)]	$\phi_{m5.3}$ (meas.)	$\phi_{m5.3}$ [Eq. (5)]	$\phi_{m10}$ (meas.)	$\phi_{m10}$ [Eq. (5)]
C1	$\infty$	0.56	$\infty$	0.48	$-\infty$	0.41
F1	$\infty$	0.60	$\infty$	0.51	$-\infty$	0.44
C2	2.56	0.75	4.12	0.65	0	0.57
C3	1.58	0.86	2.18	0.78	0	0.59
F2	0.97	0.76	1.41	0.67	0	0.59

atmospheric boundary layer (200 m in this particular case), it is not possible to apply a top-down numerical model with MO parameterization to derive the 10-m wind.

The results presented in this paper are representative for swell during the BASE period and they are common in the Baltic Sea at large. Their validity in oceanic conditions cannot be inferred from the present results. They apply to low wave height and the low wave slope of the five cases studied here (cf. Table 1), typical values being  $H_s \approx 0.25\text{--}0.6$  m and wave slope  $ak \approx 0.02\text{--}0.03$  (equals significant slope  $H_s/\lambda_d \approx 0.05\text{--}0.07$ ). This contrasts sharply with the corresponding values used in the LES of Sullivan et al. (2008):  $H_s \approx 4.5$  m and wave slope  $ak \approx 0.1$ . The qualitative agreement of basic features obtained from that simulation and from the present measurements is, however, striking, which might indicate a relatively robust mechanism, which is not critically dependent on such parameters.

The present paper has just described observed characteristics during swell in the BASE study and has not discussed possible physical mechanisms that may explain these features. An attempt to do that is made in the companion paper, Högström et al. (2009).

*Acknowledgments.* Participation of the Uppsala group was made possible by funding by the Swedish Research

Council, Grant 621-2002-5348. We wish to thank Dr Hans Bergström, Cecilia Johansson, and other colleagues at MIUU who were responsible for the measurements at Östergarnsholm.

We thank the following for various aspects of this work on land and sea: Joe Gabriele, Mike Rebozo, Henry Söderman, Teuvo Seppälä, Jari Helminen, Hannu Jokinen, and Elina Miettunen, as well as the captain and crew of the R/V *Aranda*. WD acknowledges support from the National Science Foundation, Grant OCE-0220459.

## APPENDIX

### The Effect of a Nonzero Wind/Swell Angle

Above it was shown that no effect on the mean wind profile and other atmospheric characteristics could be detected when the direction of the swell propagation  $\phi_s$  differed from that of the local wind  $\phi$  as long as  $|\phi_s - \phi| \leq 90^\circ$  (cases with significantly larger values were not encountered).

Figure A1 is a schematic picture of the situation in which the local wind is blowing perpendicular to the propagation direction of a train of two-dimensional monochromatic swell waves (i.e.,  $\phi_s - \phi = 90^\circ$ ). The wind speed  $U < c$ , the phase speed of the waves.

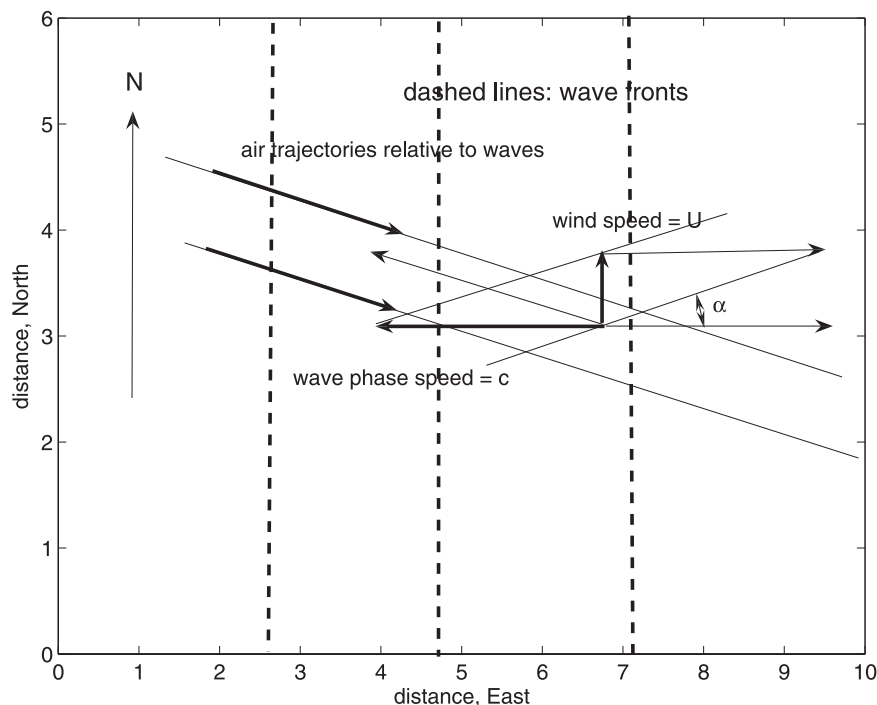


FIG. A1. Schematic picture of wind/swell geometry. The wind is from the south, with speed  $U$ ; the swell is from the east, with phase speed  $c$ . The air trajectories in a coordinate system moving with the swell waves are at an angle  $\alpha$  relative to the wave velocity vector.

The relevant wind speed from the point of view of the wave is the wind in a coordinate system moving with the wave system (cf. Höglström et al. 2009). For the geometry shown in Fig. A1, it means that the air trajectories are moving at an angle  $\alpha = \arctan(U/c)$  off the direction of wave propagation;  $\alpha$  is  $\sim 11^\circ$  for  $c/U = 5$  and  $\sim 34^\circ$  for  $c/U = 1.5$ . The geometry implies that the slant trajectories traverse a distance  $\lambda/\cos\alpha$  instead of  $\lambda$  as in the case when  $\phi_s - \phi = 0^\circ$ . For  $c/U = 5$ , this is an increase of only 2%, and for the case of  $c/U = 1.5$ , a 20% increase.

When the wind speed becomes exactly zero, the relative wind speed in a coordinate system moving with the wave system will be the only relevant wind parameter. When the wind speed is small compared with the phase speed of the swell, we may expect only minor changes to the effect controlled by the relative wind speed. This agrees with our experimental results.

## REFERENCES

- Antonia, R. A., and A. J. Chambers, 1980: Wind-wave-induced disturbances in the marine surface layer. *J. Phys. Oceanogr.*, **10**, 611–622.
- Benilov, A. Y., O. A. Kouznetsov, and G. N. Panin, 1974: On the analysis of wind wave-induced disturbances in the atmospheric turbulent surface layer. *Bound.-Layer Meteor.*, **6**, 269–285.
- Chambers, A. J., and R. A. Antonia, 1981: Wave-induced effect on the Reynolds shear stress and heat flux in the marine surface layer. *J. Phys. Oceanogr.*, **11**, 116–121.
- Davidson, K. L., and A. J. Frank, 1973: Wave-related fluctuations in the airflow above natural waves. *J. Phys. Oceanogr.*, **3**, 102–119.
- Donelan, M. A., 1987: The effect of swell on the growth of wind waves. *Johns Hopkins APL Tech. Dig.*, **8**, 18–23.
- , 1990: Air–sea interaction. *Ocean Engineering Science*, B. Le Méhauté and D. Hanes, Eds., Vol. 9, *The Sea*, Wiley-Interscience, 239–292.
- , W. M. Drennan, and K. B. Katsaros, 1997: The air–sea momentum flux in conditions of wind sea and swell. *J. Phys. Oceanogr.*, **27**, 2087–2099.
- Graber, H. C., E. A. Terray, M. A. Donelan, W. M. Drennan, J. C. Van Leer, and D. B. Peters, 2000: ASIS—A new air–sea interaction spar buoy: Design and performance at sea. *J. Atmos. Oceanic Technol.*, **17**, 708–720.
- Grachev, A. A., and C. W. Fairall, 2001: Upward momentum transfer in the marine boundary layer. *J. Phys. Oceanogr.*, **31**, 1698–1711.
- Hanley, K. E., and S. E. Belcher, 2008: Wave-driven wind jets in the marine atmospheric boundary layer. *J. Atmos. Sci.*, **65**, 2646–2660.
- Harris, D. L., 1966: The wave-driven wind. *J. Atmos. Sci.*, **23**, 688–693.
- Höglström, U., 1996: Review of some basic characteristics of the atmospheric surface layer. *Bound.-Layer Meteor.*, **78**, 215–246.
- , and Coauthors, 2008: Momentum fluxes and wind gradients in the marine boundary layer: A multi-platform study. *Boreal Environ. Res.*, **13**, 472–502.
- , A. Smedman, E. Sahleé, W. M. Drennan, K. K. Kahma, H. Pettersson, and F. Zhang, 2009: The atmospheric boundary layer during swell: A field study and interpretation of the turbulent kinetic energy budget for high wave ages. *J. Atmos. Sci.*, **66**, 2764–2779.
- Holland, J. Z., W. Chen, J. A. Almazan, and F. C. Elder, 1981: Atmospheric boundary layer. *IFYGL: The International Field Year for the Great Lakes*, E. J. Aubert and T. L. Richards, Eds., NOAA, 109–167.
- Hristov, T. S., S. D. Miller, and C. A. Friehe, 2003: Dynamical coupling of wind and ocean waves through wave-induced air flow. *Nature*, **422**, 55–58.
- Lai, R. J., and O. H. Shemdin, 1971: Laboratory investigation of air turbulence above simple water waves. *J. Geophys. Res.*, **76**, 7334–7350.
- Makova, V. I., 1975: Features of the dynamics of turbulence in the marine atmospheric surface layer at various stages in the development of waves. *Izv. Acad. Sci. USSR*, **11**, 177–182.
- Miles, J. W., 1957: On the generation of surface waves by shear flows. *J. Fluid Mech.*, **3**, 185–204.
- Pettersson, H., H. C. Graber, D. Hauser, C. Quentin, K. K. Kahma, W. M. Drennan, and M. A. Donelan, 2003: Directional wave measurements from three wave sensors during the FETCH experiment. *J. Geophys. Res.*, **108**, 8061, doi:10.1029/2001JC001164.
- Rutgersson, A., A.-S. Smedman, and U. Höglström, 2001: Use of conventional stability parameters during swell. *J. Geophys. Res.*, **106**, 27 117–27 134.
- Sjöblom, A., and A.-S. Smedman, 2002: The turbulent kinetic energy budget in the marine atmospheric surface layer. *J. Geophys. Res.*, **107**, 3142, doi:10.1029/2001JC001016.
- Smedman, A.-S., M. Tjernström, and U. Höglström, 1994: The near-neutral marine atmospheric boundary layer with no surface shearing stress: A case study. *J. Atmos. Sci.*, **51**, 3399–3411.
- , U. Höglström, H. Bergström, A. Rutgersson, K. K. Kahma, and H. Pettersson, 1999: A case study of air–sea interaction during swell conditions. *J. Geophys. Res.*, **104**, 25 833–25 851.
- , X. Guo-Larsén, U. Höglström, K. K. Kahma, and H. Pettersson, 2003: Effect of sea state on the momentum exchange over the sea during neutral conditions. *J. Geophys. Res.*, **108**, 3367, doi:10.1029/2002JC001526.
- Sullivan, P. P., J. C. McWilliams, and C.-H. Moeng, 2000: Simulation of turbulent flow over idealized water waves. *J. Fluid Mech.*, **404**, 47–85.
- , J. B. Edson, J. C. McWilliams, and C.-H. Moeng, 2004: Large-eddy simulations and observations of wave-driven boundary layers. Preprints, *16th Symp. on Boundary Layers and Turbulence*, Portland, ME, Amer. Meteor. Soc., 8.12.
- , —, T. Hristov, and J. C. McWilliams, 2008: Large-eddy simulations and observations of atmospheric marine boundary layers above nonequilibrium surface waves. *J. Atmos. Sci.*, **65**, 1225–1245.
- Vickers, D., and L. Mahrt, 2003: The cospectral gap and turbulent flux calculations. *J. Atmos. Oceanic Technol.*, **20**, 660–672.
- , and —, 2006: A solution for flux contamination by mesoscale motions with very weak turbulence. *Bound.-Layer Meteor.*, **118**, 431–447.
- Volkov, Yu. A., 1970: Turbulent flux of momentum and heat in the atmospheric surface layer over a disturbed sea-surface. *Izv. Acad. Sci. USSR*, **6**, 770–774.